SWIMMING WITH THREE-DIMENSIONAL FLAGELLAR BENDING WAVES

Charles J. Brokaw

Division of Biology, California Institute of Technology, Pasadena CA 91125 USA
E-mail: brokawc@its.caltech.edu

Abstract – Computer simulation methods have been developed for study of bending wave generation by model flagella that can bend in three dimensions. Helical bending wave generation appears to be the default result obtained with the simplest possible mechanism for controlling activity of the dynein motor enzymes that propel a flagellum. The new computer simulation methods allow a more realistic comparison of swimming by helical or planar bending waves. They confirm earlier conclusions that for small uniflagellate cells such as spermatozoa, planar bending waves are better than helical bending waves. Given the basic radial symmetry of flagellar structure, generation of planar bending waves requires the evolution of more complex control mechanisms.

I. Introduction

The eukaryotic flagellum is a cylindrical structure containing a cytoskeleton referred to as the axoneme. The axoneme contains all of the machinery required for generation of appropriate bending patterns by flagella and cilia. The primary component of the axoneme is a ring of equally-spaced outer microtubular doublets, forming the cylindrical surface of the axoneme. In most cases, these doublets appear to be identical and are nine in number. Each outer doublet supports rows of the motor enzymes known as dyneins. One row, containing the inner arm dyneins, contains a complex of about seven distinct dyneins, repeating at 96 nm intervals along the length. The inner arm dyneins are required for initiation and propagation of bending. A second row, present in most axonemes, contains one type of dynein, repeating at 24 nm intervals along the length. These outer arm dyneins act as amplifiers, increasing the frequency of beating and probably generating the majority of the power output. Dyneins generate sliding between microtubular doublets, which can be converted into bending of the axoneme by local differences in dynein activation or sliding resistance along the length of the flagellum.

We have very little information about the control mechanisms that operate within flagella to produce local differences in dynein activation or sliding resistance, in order to generate appropriate bending patterns. Speculation about control mechanisms has been assisted by computer models that can generate bending patterns that result from hypothetical control mechanisms. These computer simulations were originally focused on flagellar models that were restricted to planar bending. A simple switching of dynein activation by the local curvature of the flagellum was found to be sufficient to provide a mechanism for flagellar oscillation and propagation of bending waves along the flagellum [1].

This computer simulation approach has recently been expanded to deal with flagellar models that can bend in three dimensions [2]. Local switching of dynein activation by the curvature of each doublet is sufficient to establish a pattern of dynein activation referred to as "doublet metachronism". In this pattern, regions of dynein activation propagate along each doublet, with a phase shift of approximately $2\pi/9$ radians between each adjacent pair of doublets. When each outer doublet is identical, doublet metachronism is the default result and the appropriate activation pattern for the production of a helical bending wave. However, most sperm flagella generate planar bending waves. We need to understand why and how they do this.

II. Methods

The method for simulation of flagellar movement uses a computer to obtain numerical solutions to the moment balance equation for a flagellum. This equation is the partial differential equation that balances active bending moments generated within the flagellum against the bending moments resulting from structural and external resistances to bending. These moments are functions of the shape of the flagellum, the rate of change of shape, and the current state of the active moment generating system. The rates of change of shape, at discrete intervals along the length of the flagellum, are the unknown variables. After solving the equation, these rates are used to update the shape, and the process is repeated through time.

This computer simulation method was initially developed for a two-dimensional model of a flagellum, which was restricted to bending in a plane [1]. The shape of the flagellum was described by its curvature at discrete points along the length, and the rates of change of curvature, $d\kappa/dt$, were the unknown variables. The method has now been extended to a model that can bend in three dimensions [2]. In three dimensions, the curvature and rate of change of curvature are vector variables, with x, y and z components in the local coordinate system at each point along the length of the flagellum. In current models, shear forces generated along each of the outer microtubular doublets, usually 9 in number, are developed and incorporated independently. Active

bending moments are obtained by integrating active shear forces along the length. No attempt is made to consider the forces that maintain the position of the outer doublets in the flagellar cross-section. Bending, twist, and internal sliding are the only allowed motions, and these are coupled because bending results from differences in sliding at positions along the length.

Active shear forces for each outer doublet can be obtained by stochastic modelling of the behavior of each individual dynein motor [2,3,4,5]. Since a typical flagellum contains tens of thousands of individual dynein motors, this is computationally slow, and for many purposes it is valuable to obtain active shear forces from a simple mathematical model that incorporates the property that the active shear force decreases with sliding velocity [2,6]. Results in this paper have been obtained with this simplified method for active shear force.

External viscous resistances are incorporated using the approximate method introduced by Gray and Hancock [7] and improved by Lighthill [8]. This method is known as the resistance coefficient method. It assumes that the viscous resistance on any segment of the model can be obtained by multiplying the velocity components by resistance coefficients that are the same at every point along the length of the flagellum. Propulsion results from the fact that the resistance coefficients are 1.8 times larger for movement normal to the length than for movement parallel to the length.

In the previous paper on three-dimensional models [2], the method used for computing the moments resulting from external viscous resistance was not sufficiently accurate. The problem arises in computing the velocity, relative to the external fluid, of a segment *j* of the flagellum caused by rate of change of curvature at each joint *k*. In two dimensions, this can be done accurately by multiplying the local rate of change of curvature by the distance between joint *k* and segment *j*. This lever arm distance can be obtained from the current shape of the flagellum [1]. In three dimensions, the rate of change of curvature is a vector in the local coordinate system of the flagellum, and it must be transformed to the external coordinate system of the surrounding fluid before being multiplied by the lever arm distance. In Equation 14 of the previous paper [2], the local rate of change of curvature at joint *k* was transformed using the transformation matrix A[*k*]. This did not give accurate velocities. However, if the transformation is performed using 0.5*(A[*k*] + A[*k*+1]), sufficiently accurate velocities are obtained. The rationale for this adjustment is discussed in detail elsewhere [9]. The results in the remainder of this paper are the first results presented using this new method.

In order for these computer methods to generate more or less realistic flagellar motions, some form of control of the dynein-generated shear moment is required. In particular, at any position along the length, dyneins on one side of the axoneme must be inactive while dyneins on the other side are active. This is required to prevent a situation where all of the dyneins are antagonizing each other and producing no useful bending. The models examined here use a simple form of local curvature control, in which dyneins on each doublet respond to the local curvature of that doublet. Dyneins on a doublet become active when the local curvature exceeds a critical value, and remain on until the local curvature of that doublet exceeds the critical value in the opposite direction. The hysteresis in this control loop provides a basis for oscillation. In a flagellar model that can bend in three dimensions, this form of local control is sufficient to establish doublet metachronism, in which regions of dynein activation and inactivation propagate along the length with a phase shift of approximately $2\pi/9$ radians between adjacent doublets [2]. The cycle frequency of the model is the repeat frequency of the doublet metachronism pattern, and also the frequency of rotation of the curvature vector in the local x,y plane of the flagellum.

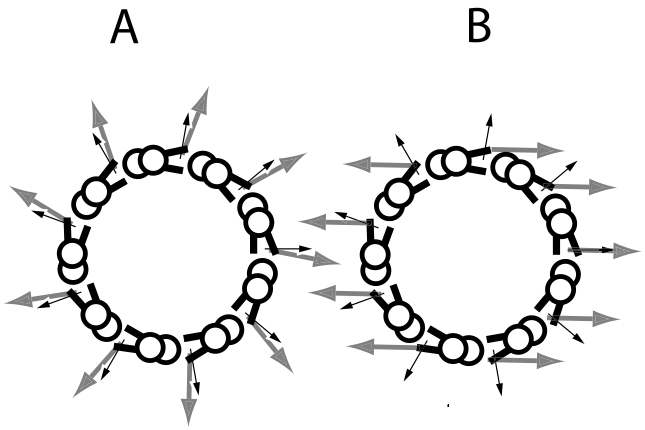

Fig. 1. Diagrams showing the positions of outer doublets in the axonemal cross-section. Thin black arrows indicate the direction of the shear moment vector produced by the dyneins on each doublet. Thick gray arrows indicate a possible direction for the controlling curvature for each doublet. In A, each doublet is identical. In B, the controlling curvature directions have been modified so that planar bending will be generated.

Forward velocity for planar bending patterns is measured by the change in position of the base of the flagellum in one bending cycle. This method is difficult to apply to three dimensional bending, because the frequency of rotation of the helical pattern is not equal to the cycle frequency. Forward velocity for helical bending patterns is estimated by the average velocity of the base in the local z coordinate direction. These velocities were computed for 4 bending cycles, after stabilization of the bending pattern.

Parameters for a specific example -- Results for the example used for this paper were obtained with the following parameters:

The structure of the flagellum is defined by using

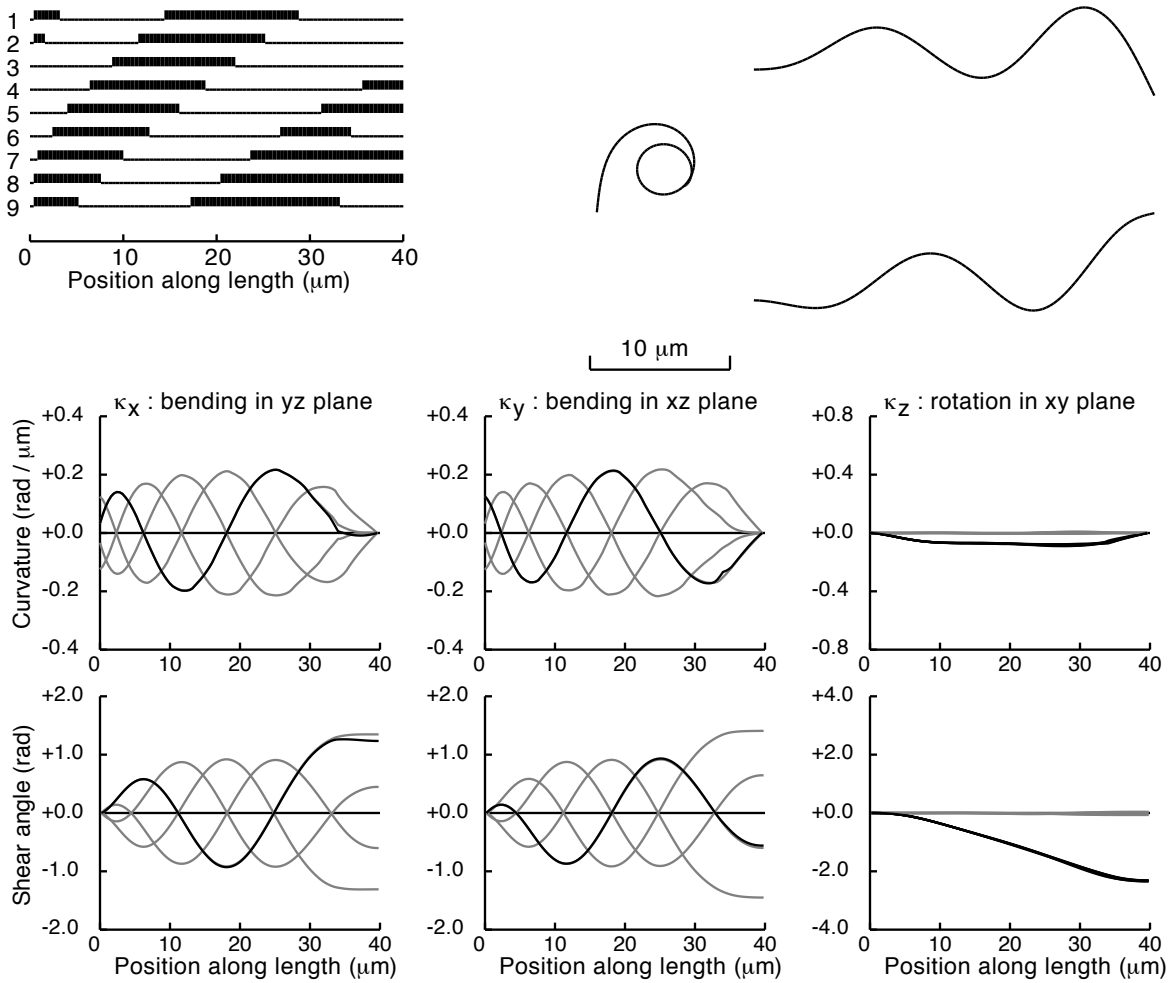

Fig. 2. Output from a typical computation using a simple mathematical model for dynein activity, with identical control of dyneins on each outer doublet, as indicated in Fig. 1A. Normal external viscosity, with no load at the base of the flagellum. Parameters for this model are given in Methods. The diagram in the upper left shows regions of active and inactive dynein on each outer doublet, at the end of the computation. Three diagrams in the upper right show the shape of the flagellum at the end of the computation, as projections on the YZ, XY, and XZ planes (from top to bottom). The lower plots show curvature and shear angle at 0.25 cycle time points in the last cycle of bending, using black curves at the final time point and gray curves at the earlier time points. The plots for rotation in the xy plane use black curves to show total rotation (twist + writhe) and gray curves to show twist. The frequency is 41 cycles per sec.

---

9 outer doublets, with a center to center spacing of 60 nm, placing them in a circular array with a diameter of 175 nm (Fig. 1). In the absence of external forces, these doublets run straight along the axonemal cylinder, without twist. This matches the geometry of the majority of simple flagella and cilia. Simple sperm flagella typically range in length from 30 to 50 μm. A length of 40 μm is used for this example. The standard value of elastic bending resistance of 2.0×10^8 pN nm^2 is consistent with various experimental measurements of axonemal and microtubule stiffness [6]. Elastic shear resistance, which might be provided by interdoublet linkages other than dyneins, is not a necessary component, but contributes to uniformity of bend amplitude along the length [2]. A relatively low value of 3 pN per doublet for the non-linear elastic shear resistance constant is used in this example. The elastic twist resistance is 2.2 times the elastic bending resistance, as calculated for the simplest axonemal model by Hines and Blum [10].

The active shear moment generated along each doublet is generated by a simple mathematical model with three parameters [6]. The maximum shear moment at 0 sliding velocity is 6 pN nm/nm. Since the wave number increases with the ratio of maximum shear moment to elastic bending resistance, as in two-dimensional models [6], this value is chosen empirically to give a wave number in the desired range.

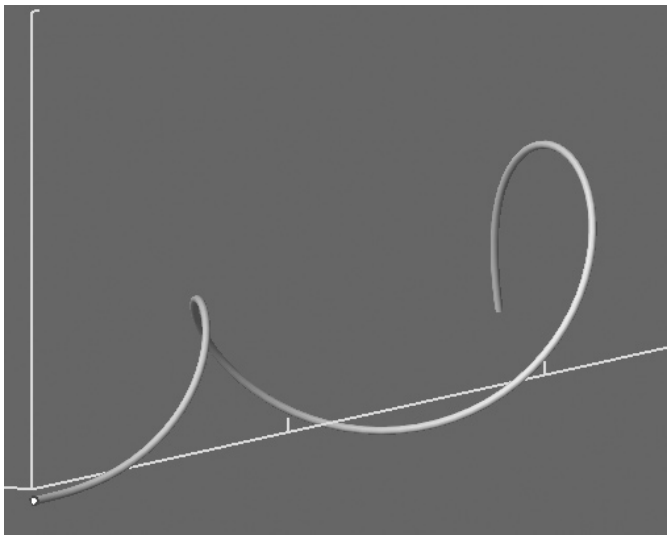

Fig. 3. Three dimensional view of the shape of the flagellar model at the end of the computation illustrated in Fig. 2. The vertical Y axis length is 10 μm. The Z axis has ticks at 10 μm intervals.

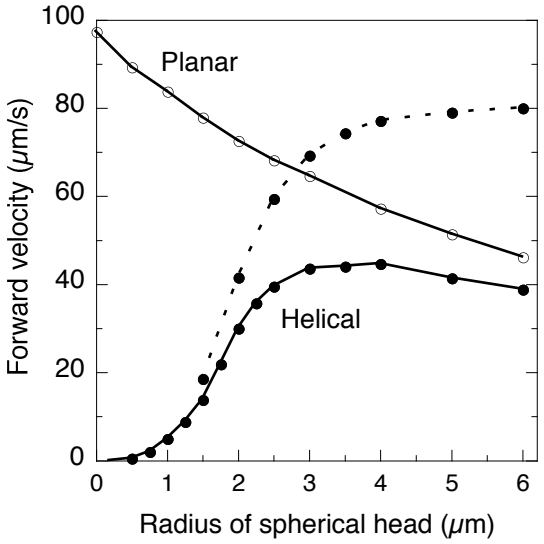

Fig. 4. Results of computer simulations using the model of Fig. 2, with the addition of a spherical viscous load at the base of the flagellum. The lower two curves, with solid points, show velocities obtained with the dynein contol protocol shown in Fig. 1A, which produces helical bending waves. The curve with a dashed line shows the results that would be obtained if the spherical viscous load only resists rotation, without resisting linear movement. The upper curve, with open circles, shows velocities obtained with the dynein control protocol shown in Fig. 1B, which produces planar bending waves.

The stiffness of the active shear moment system is given a value of 4, which means that a sudden shear step of 0.25 rad, or 15 nm, will reduce the moment to 0 [6]. The effective stiffness of myosin motors in skeletal muscle is 2-4 times stiffer than this value, but no information is available for dynein. The recovery rate constant has a value of 1300 s^{-1}, which gives an appropriate frequency. In the steady state, the force generated by this model decreases linearly with increasing sliding velocity, to 0 at a sliding velocity equal to the rate constant divided by the stiffness, or 325 rad s^{-1}.

The control of the active shear system involves two parameters, which primarily regulate the pitch angle of the helical bending pattern [2]. The critical curvature at which switching occurs is 0.12 rad μm^{-1}. The angle between the azimuthal directions of moment and controlling curvature (see Fig. 1A) for each doublet is 0.16 rad. The sign of this angle parameter determines the handedness of the helix [2].

The standard viscosity corresponds to a tangential viscous drag coefficient of 2.16×10^{-9} pN s nm^{-1} [2, 6]. Computations were performed with the length of the flagellum divided into 100 equal segments (length 0.40 μm) and 400 time steps per bending cycle.

III. Results

Using a simple form of local curvature control of dynein activity (described in Methods), the three-dimensional flagellar models can generate quasi-helical bending patterns. Figs. 2 and 3 show results at the end of a typical computation. The shape of the flagellum is not a pure helix, because bending is initiated at the basal end in a manner that keeps the basal end close to the helix axis, rather than on a cylindrical surface. For biologically useful swimming, this is a much more satisfactory solution. Results very similar to those shown in Fig. 2 are obtained for a model operating in the absence of any external viscous resistance. Operation at 0 viscosity is possible because the mathematical formulation used for generating active dynein shear forces is such that the shear force decreases linearly with sliding velocity, as if a viscous resistance were present to reduce the net shear force. In contrast to the situation with two-dimensional bending [6], addition of external viscosity has relatively little effect on the helical movement. This is because the viscous resistance to rotation of the flagellum around its longitudinal axis is very low, compared to resistance to movement through the fluid. Consequently, this rotation becomes the primary movement, and minimizes the lateral movement of the flagellum against the surrounding fluid. As a result, little or no thrust is generated, and the forward velocity is close to 0 [11,12].

A flagellum is normally attached to a cell body that increases the resistance to rotation and thereby allows a helical bending wave to generate thrust, propelling the cell body. Fig. 4 shows results computed for the same model as Fig. 2, at normal external viscosity, with a spherical load at the base of the flagellum. As the radius of the load is increased, the

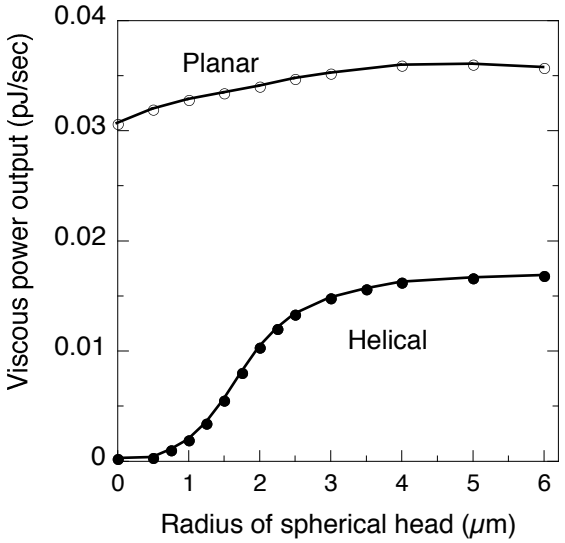

Fig. 5. Results of computer simulations using the model of Fig. 2, with the addition of a spherical viscous load at the base of the flagellum. These curves show the calculated power output against the viscous resistances acting on the flagellum and the spherical load, for various values of spherical load radius.

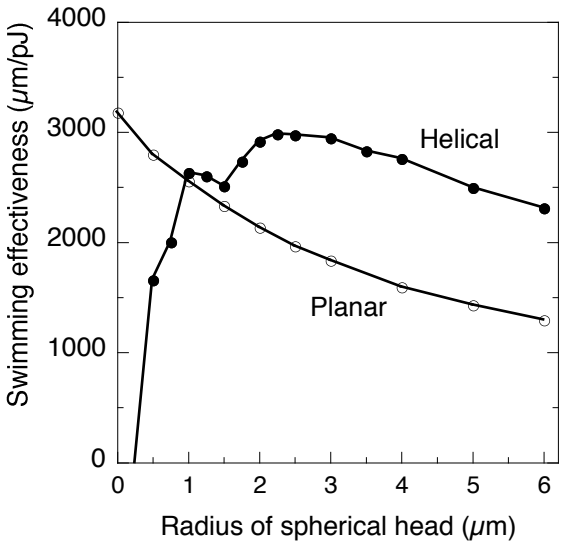

Fig. 6. Results of computer simulations using the model of Fig. 2, with the addition of a spherical viscous load at the base of the flagellum. These curves show the biological effectiveness of the swimming movements, calculated by dividing the forward swimming velocity by the viscous power output.

forward swimming velocity increases. The velocity would asymptotically approach a limit as the rotation is completely suppressed (dashed line in Fig. 4), but the spherical load also introduces a resistance to forward progression, so that the forward velocity eventually starts to decrease.

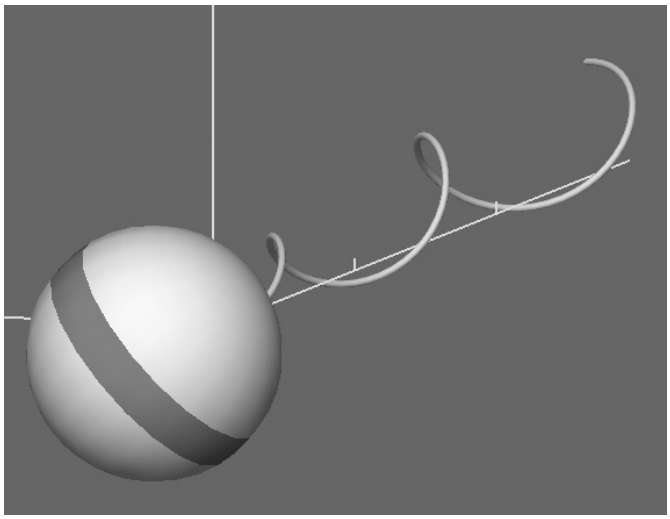

Fig. 7. Three dimensional view of the shape of the flagellar model at the end of a computation. Like the example in Fig. 2, except that a spherical head with a radius of 3 μm is placed at the base of the flagellum. The vertical Y axis length is 10 μm. The Z axis has ticks at 10 μm intervals.

This is not a new insight, but has been demonstrated in previous works [12]. The difference here is that in previous work, the flagellum was assumed to generate a perfect helix, with constant frequency, amplitude, and wavelength. The results in Fig. 4 were obtained with a more biologically realistic model, with the dynein motor parameters held constant, while the shape and frequency of the bending motion were allowed to adjust to the increased load. Additionally, the pattern of bend initiation at the basal end of the flagellum is more biologically realistic. However, these results are still based on the very approximate resistance coefficient hydrodynamics, in which the distortion of the local fluid velocities on the flagellum by the movement of the large spherical load is not considered.

Fig. 4 also shows, for comparison, the effect of adding a spherical load at the basal end when the model is generating planar bending waves instead of helical bending waves. The planar bending waves were obtained with exactly the same model that generated helical bending waves, except for a change in the way that the dyneins are controlled. As shown, when a model is generating planar bending waves, it achieves its maximum forward swimming velocity when no load is present. The velocity decreases as the radius of the spherical load is increased. Again, this is not a new result; a somewhat similar comparison is shown by Chwang and Wu [12]. These new results in Fig. 4 are from biologically more realistic computations, but the general conclusion is the same.

These computations also provide results for the power dissipation against the external viscous resistance. These results are shown in Fig. 5. Note that this is the power output of the flagellar model, not its power input or fuel consumption. Results for the power input, or ATP consumption, can be computed using the more complex models that incorporate

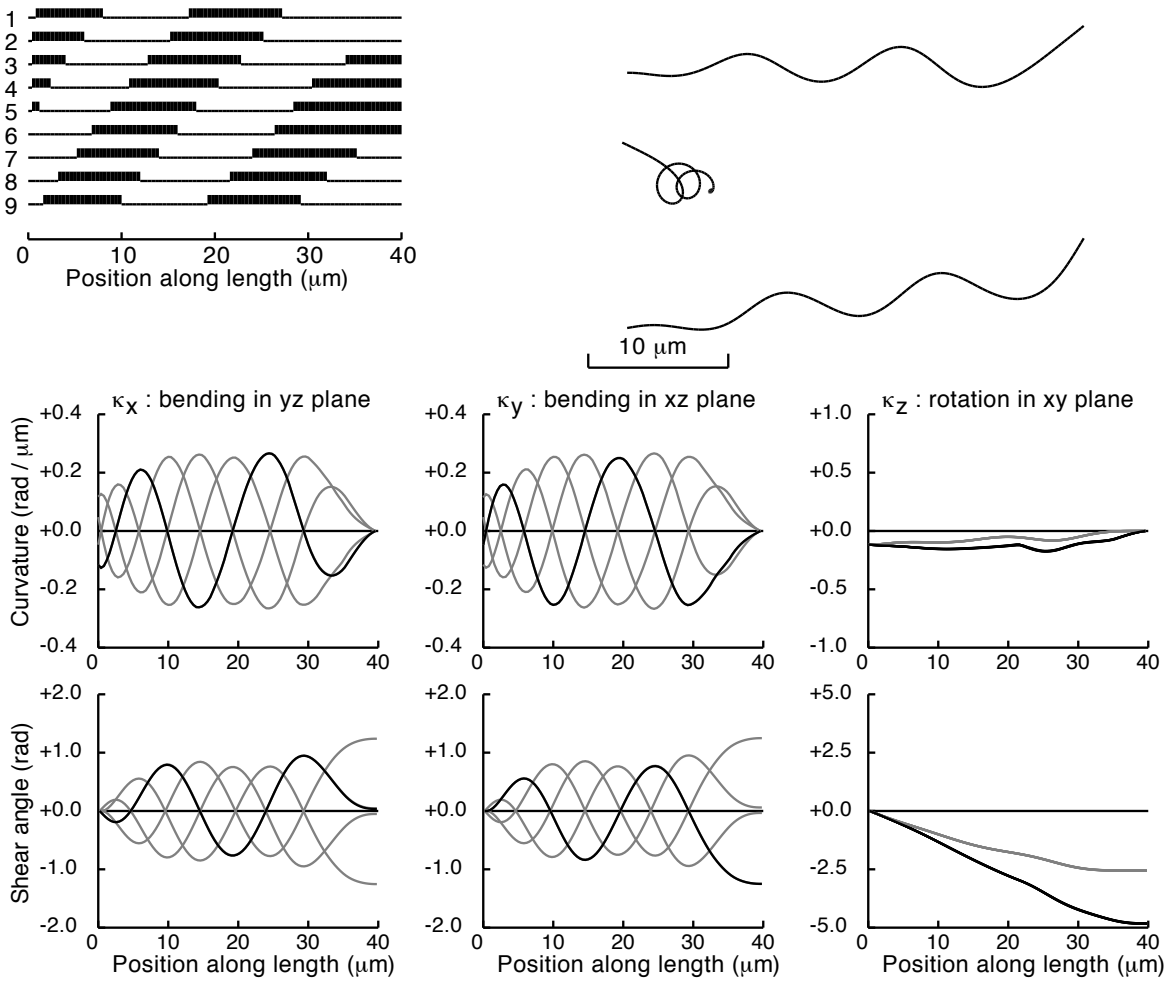

Fig. 8. Output from a computation similar to Fig. 2, except that a spherical head with a radius of 3 μm is placed at the base of the flagellum. The frequency is 47 cycles per sec.

---

kinetics for the individual dyneins, but are rather hypothetical because we have very little information about the parameters of dynein function.

Fig. 6 shows the biological effectiveness of the movement, obtained by dividing the forward velocity by the power. This is not the hydrodynamic efficiency, which would be the power used to push the load through the viscous fluid, divided by the total viscous power. For something like a sperm cell, the effectiveness is a guide to how it should be designed to obtain maximum speed for a given power capability, or to obtain maximum distance from a given fuel supply.

Fig. 7 shows the shape of the flagellum computed with a spherical load at the base of the flagellum, with a radius of 3 μm. More detailed results for this case are shown in Fig. 8. There is an obvious increase in wave number corresponding to the addition of almost one complete helical turn. This is accompanied by an increase in frequency. Most of these changes occur when the radius is increased from 1.0 to 2.5 μm; these changes are reflected in the complexity of the effectiveness curve in this region (Fig. 6).

Writhe and twist -- Closer inspection of Fig. 2 or Fig. 8 reveals that the wave number of the helical shape is greater than the wave number shown by the plots of curvature or shear angle along the length [2]. In each turn of the helix, the curvature vector must rotate by 2π radians around the axis of the helix. The major portion of this rotation of the curvature vector results from the torsion, defined as rotation of the curvature vector in the x,y plane of the local x,y,z coordinate system of the flagellum. There is an additional rotation of the local x,y,z coordinate system which accumulates as the flagellum is bent by the curvature. This additional rotation is the writhe of the curve, and is shown in Fig. 2 by the heavy black lines in the plots of rotation in the x,y plane. The method for calculating the rotation of the local x,y,z coordinate system is given in [9]. When a load is present at the base of the flagellum, an

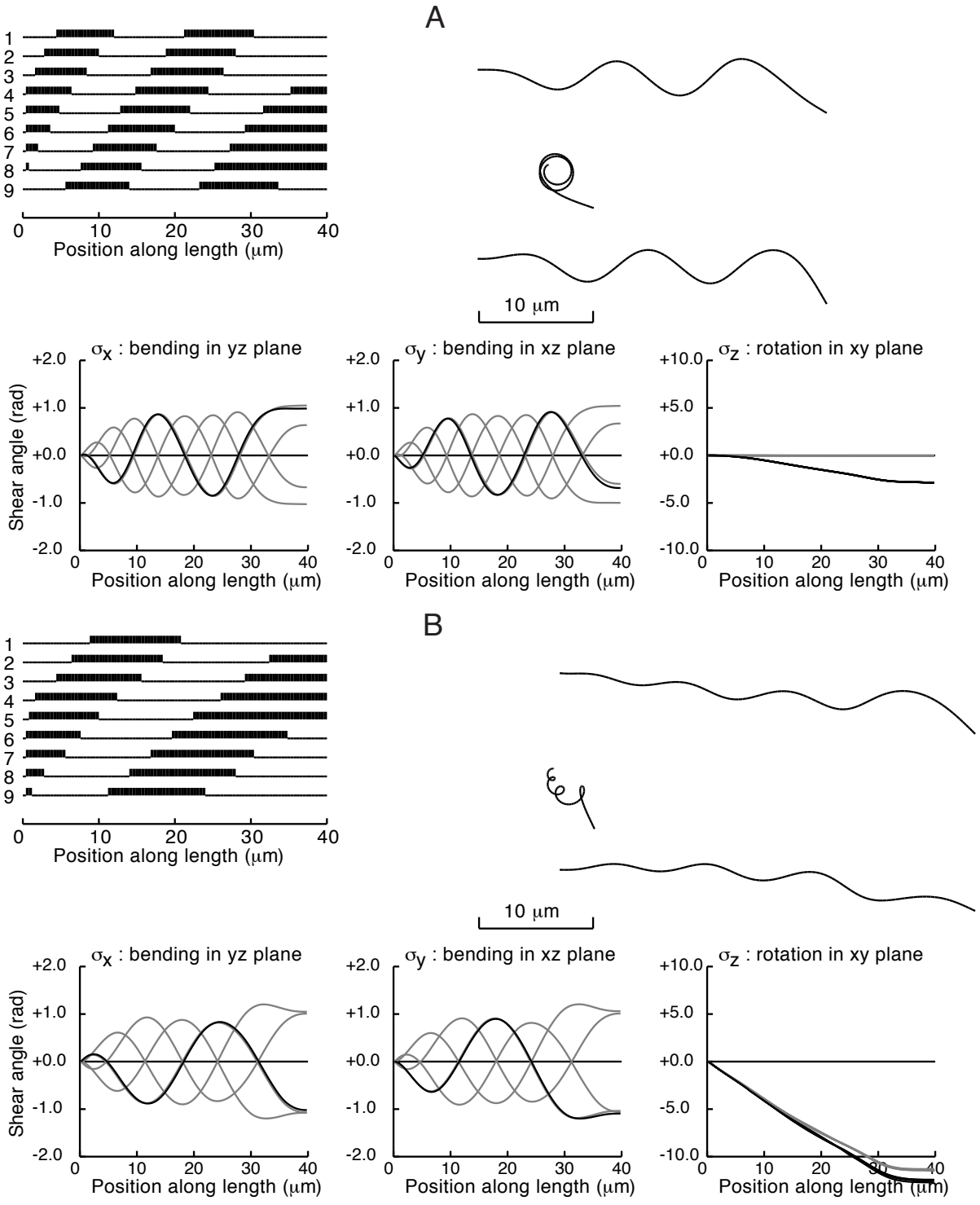

Fig. 9. Output from computations similar to Fig. 5, with a spherical head with a radius of 3 μm at the base of the flagellum. In A, the elastic twist resistance has been increased by a factor of 100, to 440×10^8 pN nm^2. The frequency is 48 cycles per sec. In B, the elastic twist resistance has been decreased by a factor of 10, to 0.44×10^8 pN^2. The frequency is 42 cycles per sec. Note the change in the scale of the rotation plots, compared to Fig. 8.

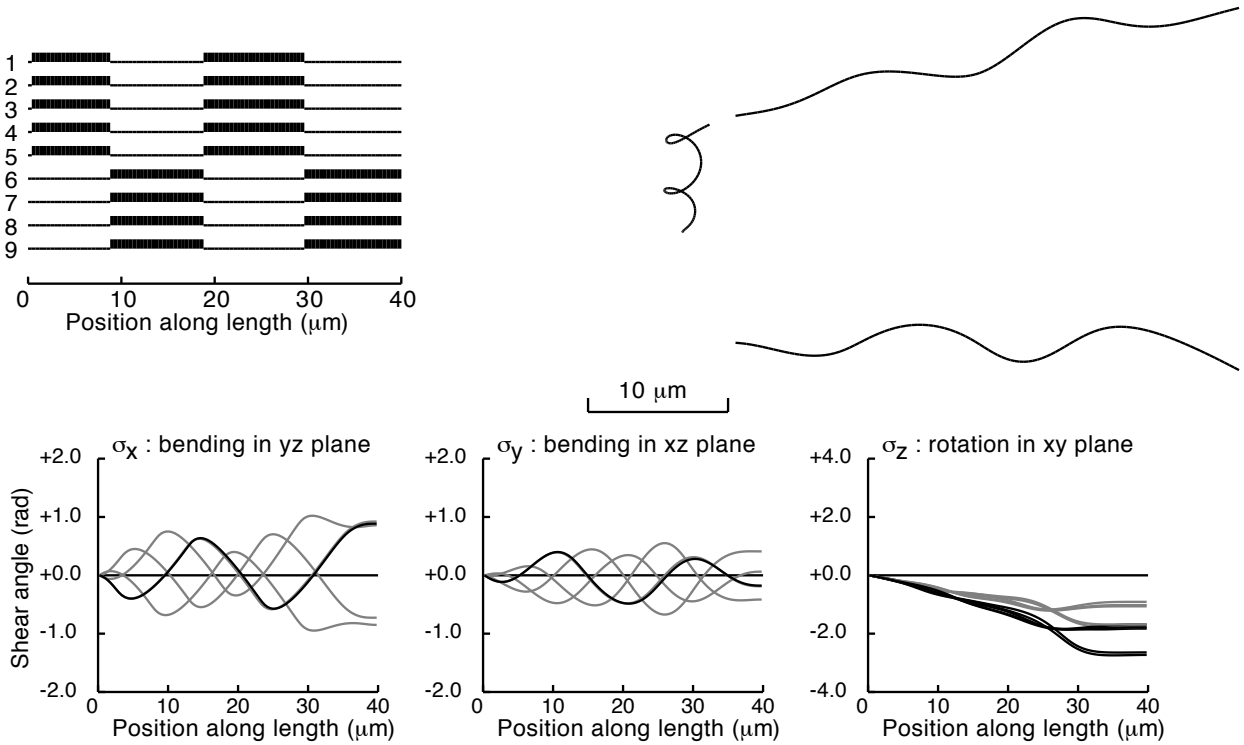

Fig. 10. Output from a computation similar to those used to obtain data for planar bending, in Figs. 4 - 6, using the control protocol illustrated in Fig. 1B, and a spherical load with a radius of 1 μm at the base of the flagellum. In this case, the external viscosity is increased to 4 times the standard viscosity. The frequency is 41 cycles per sec.

additional rotation results from twisting of the flagellum, against its elastic twist resistance. In Fig. 8, this twist rotation is shown by the gray lines in the plots of rotation in the x,y plane. The black lines in these plots show the total rotation of the local x,y,z coordinate system, including both twist and writhe. These plots show that the total rotation increases when there is a load at the base of the flagellum.

The role of twist is seen more clearly by varying the elastic twist resistance of the model. The value of elastic twist resistance used for Figs. 2-8, 4.4×10^8 pN nm^2, was a standard value calculated on the assumption that the outer doublet microtubules have isotropic properties [10]. Computations (not shown) were performed with lower (2.2×10^8 pN nm^2) and higher values (8.8×10^8 pN nm^2). There was little detectable difference between the plots of curvature and shear angle in the local coordinate system, at these values of elastic twist resistance. There were small but noticeable differences in total rotation and wave number. Results obtained with more extreme changes in elastic twist resistance are shown in Fig. 9. With a very high value of elastic twist resistance (Fig. 9A), twist is essentially eliminated, and all of the rotation of the local coordinate system results from writhe, as in the cases where there is no load at the base of the flagellum (Fig. 2). The differences between the wave shape and motion in Fig. 9A and Fig. 8 are small. There is a small increase in peak curvature, which causes an increased helix pitch angle and helix radius, leading to an increase of about 12% in swimming velocity. The normal value of twist resistance calculated by Hines and Blum [10] appears to be sufficient to eliminate deleterious effects of twist, and there would be no great benefit in evolving a greater twist resistance. With a very low value of elastic twist resistance (Fig. 9B), the total rotation of the local coordinate system increases from about 5 rad to about 12 rad, but the amount resulting from writhe falls from 2.5 rad to about 1.25 rad. The increased total rotation increases the disparity between the wave numbers indicated by the plots of shear angle along the length and the wave number indicated by the helical shape. The helical radius is significantly reduced, and the swimming velocity falls to less than half the value obtained from the computation in Fig. 8.

Instability of planar bending at increased viscosity -- Fig. 10 shows results from a computation with a model incorporating the appropriate control for production of planar bending waves, shown in Fig. 1B. This model is the same model used to produce the planar results in Figs. 4-6, with a spherical load radius of 1 μm. However, for Fig. 10, the external viscosity has been increased by a factor of 4. Planar bending is unstable under these conditions, and the bending changes to a complicated three-dimensional pattern that is only approximately helical. The pattern of dynein activation remains appropriate for planar bending, without converting to doublet metachronism. This conversion to a quasi-helical bending pattern was suppressed

by increasing the elastic bending resistance in the x,z plane by a factor of 4, but was not suppressed by increasing this bending resistance by a factor of 2 (not shown). The frequency of the quasi-helical pattern was 41 cycles per sec, compared to 26.8 cycles per sec for the planar pattern obtained with increased x,z plane bending resistance. In other examples, both left- and right-handed patterns were obtained.

IV. Discussion

The modelling results shown in Figs. 2 to 6 are only for one model with a particular set of parameters. Results have been computed for models with a variety of parameters, and the results are qualitatively the same. The conclusion is always that, for something like a sperm cell with a small head, planar bending waves are better than helical bending waves. Again, this is not a new insight, but was realized by Sir James Gray more than 50 years ago [11]. What was not realized at that time is that it appears to be much easier for a flagellum to produce helical waves than planar waves. In models such as these, helical bending waves are the default result when each of the 9 outer doublets is identical, except for its position in the axonemal cross-section. The direction of the controlling curvature is the same for each doublet, when measured relative to the azimuthal position of each doublet (Fig. 1A). Each doublet is independent, except for its mechanical interactions with the rest of the axoneme. Since this is the simplest possible situation and result, something more complicated must have evolved to generate stable planar bending. The results for planar bending in Figs. 4-6 were obtained by redesigning the control system as shown in Fig. 1B. In this case, the directions of the controlling curvature for each outer doublet are different, so that doublets 1 to 5 are controlled by curvature in one direction, and doublets 6 to 9 are controlled by curvature in the opposite direction. This specification is easy to put into the computer model, and in some cases gives an excellent planar result. However, there is interesting experimental evidence that suggests that real flagella have not adopted this "hard-wired" solution.

There is evidence for an important role for the "central pair" of microtubules and associated structures in the interior of the axoneme in regulating planar bending [13]. Most sperm flagella contain a central pair complex, and produce planar bending waves. Eel spermatozoa lack the central pair complex, and produce helical bending waves [14]. In horseshoe crabs, the central pair is present in the sperm flagella of the American species, which produce planar bending waves. The central pair is absent in the sperm flagella of the Asian species, which produce helical bending waves [15].

One of the exceptions to this correlation has been provided by observations of tunicate and sea urchin sperm flagella. These flagella normally produce planar bending waves, but under certain high viscosity conditions have been observed to switch to helical bending [16, 17]. These observations suggest that if there is a mechanism that behaves like the control mechanism indicated in Fig. 1B, it must be able to be converted so that it operates like the control mechanism indicated in Fig. 1A under some extreme conditions. However, the result shown in Fig. 10 may indicate that this type of conversion is not required for the generation of quasi-helical bending waves. A detailed modelling of the results obtained with sea urchin sperm flagella at very high viscosities [17] will require more advanced methods for calculation of external viscous resistances, so that the interaction between closely spaced gyres of a helix can be incorporated.

By capturing the head of a sea urchin spermatozoon in a micropipette, and vibrating the micropipette laterally, the frequency and bending plane of the flagellum can be altered [18]. Extensive rotation of the bending plane can be induced, apparently without rotation of the entire axoneme [19]. When the applied vibration is turned off, the bending plane rotates back towards its original orientation. These observations suggest that the plane of flagellar bending can be determined by mechanical factors. One possibility is that the plane of flagellar bending may correspond to the plane of least bending resistance. Early on, the correlation between the bending plane and the orientation of the central pair suggested that the direction of least bending resistance, and consequently the bending plane, was determined physically by the central pair microtubule structures. The mechanical effect of the central pair microtubules on the direction of least bending resistance is probably small [10], but many flagella have additional structural modifications that appear to enhance the anisotropy of bending resistance.

The possible role of bending resistance differences in determining planar bending has been examined by computer simulations with the model that is able to bend in three dimensions. These simulations demonstrate that for reasonable variations in bending resistance, a minimum bending resistance in one plane is not sufficient to establish planar bending [2]. It is still possible that a minimum bending resistance in one plane might determine the plane of bending if the flagellum is committed to planar bending, but a model that separates the commitment to planar bending from the determination of the bending plane has not been found. The control mechanism illustrated in Fig. 1B does not have this dualism. The simulations such as Fig. 10 also show that even the hard-wired control mechanism illustrated in Fig. 1B is unable to produce stable planar bending at higher than normal viscosities, unless it is assisted by large increases in twist resistance or out-of-plane bending resistances [2]. Evidence for such resistances is lacking. A much more dynamic control mechanism may be involved in maintaining planar bending.

V. Conclusion

Because planar bending can easily produce higher swimming velocities than helical bending, there must have

been strong selective pressures favoring the evolution of planar bending waves for sperm flagellar motility. Although, to us, planar bending waves seem simpler than three-dimensional bending waves, we can now recognize that biologically, the axoneme is an ideal design for generating helical bending waves by a very simple control mechanism. The capability for generating planar bending waves that can remain stable even at increased viscosities appears to require much more sophisticated control mechanisms, which at present are unknown to us.

References

[1] C. J. Brokaw, “Computer simulation of flagellar movement I. Demonstration of stable bend propagation and bend initiation by the sliding filament model” *Biophys. J.*, vol. 12, pp. 564-586, 1972.

[2] C. J. Brokaw, “Computer simulation of flagellar movement VIII: Coordination of dynein by local curvature control can generate helical bending waves”, *Cell Motil. Cytoskel.*, vol. 53, pp. 103-124, 2002.

[3] C. J. Brokaw and D. R. Rintala, “Computer simulation of flagellar movement III. Models incorporating cross-bridge kinetics”, *J. Mechanochem. Cell Motil.*, vol. 3, pp. 77-86, 1975.

[4] M. Hines and J. J. Blum, “Bend propagation in flagella. II. Incorporation of dynein cross-bridge kinetics into the equations of motion”, *Biophys. J.*, vol. 25, pp. 421-442, 1979.

[5] C. J. Brokaw, “Models for oscillation and bend propagation by flagella”, *Symp. Soc. Exptl. Biol.*, vol. 35, pp. 313-338, 1982.

[6] C. J. Brokaw, “Computer simulation of flagellar movement VI. Simple curvature-controlled models are incompletely specified” *Biophys. J.*, vol. 48, pp. 633-642, 1986.

[7] J. Gray and G. J. Hancock, “The propulsion of sea-urchin spermatozoa”, *J. Expt. Biol.*, vol. 32, pp. 802-814, 1955.

[8] J. Lighthill, “Flagellar hydrodynamics”, *Soc. Ind. Appl. Math. Rev.*, vol. 18, pp. 161-230, 1976.

[9] C. J. Brokaw, (2002) "Torsion, twist, and writhe: the elementary geometry of axonemal bending in three dimensions". [Online] Available at: www.its.caltech.edu/~brokawc/Suppl3D/TTWcomb.pdf

[10] M. Hines and J. J. Blum, "Three-dimensional mechanics of eukaryotic flagella", *Biophys. J.*, vol. 41, pp. 67-79, 1983.

[11] J. Gray, "Undulatory propulsion", *Quart. J. Microscop. Sci.* , vol. 94, pp. 551-578, 1953.

[12] A. T. Chwang and T. Y. Wu, "A note on the helical movement of micro-organisms", *Proc. Roy. Soc. Lond. B*, vol. 178, pp. 327-346. 1971.

[13] C. K. Omoto, I. R. Gibbons, R. Kamiya, C. Shingyoji, K. Takahashi, and G. B. Witman, "Rotation of the central pair microtubules in eukaryotic flagella", *Mol. Biol. Cell*, vol. 10, pp. 1-4, 1999.

[14] B. H. Gibbons, B. Baccetti, and I. R. Gibbons, "Live and reactivated motility in the 9+0 flagellum of Anguilla sperm", *Cell Motil.*, vol. 5, pp. 333-350, 1985.

[15] S. Ishijima, K. Sekiguchi, and Y. Hiramoto, "Comparative study of the beat patterns of American and Asian horseshoe crab sperm: evidence for a role of the central pair complex in forming planar waveforms in flagella", *Cell Motil. Cytoskel.*, vol. 9, pp. 264-270, 1988.

[16] C. J. Brokaw, "Effects of increased viscosity on the movements of some invertebrate sperm flagella", *J. Exptl. Biol.*, vol. 45, pp. 113-139, 1966.

[17] D. M. Woolley and G. G. Vernon, "A study of helical and planar waves on sea urchin sperm flagella, with a theory of how they are generated", *J. Exptl. Biol.*, vol. 204, pp. 1333-1345, 2001.

[18] I. R. Gibbons, C. Shingyoji, A. Murakami, and K. Takahashi, "Spontaneous recovery after experimental manipulation of the plane of beat in sperm flagella", *Nature*, vol. 325, pp. 351-352, 1987.

[19] C. Shingyoji,J. Katada, K. Takahashi, and I. R. Gibbons,"Rotating the plane of imposed vibration can rotate the plane of flagellar beating in sea-urchin sperm without twisting the axoneme", *J. Cell Sci.*, vol. 98, pp. 175-181, 1991.